# FLIGHT PLANNING FOR THE INTERNATIONAL SPACE STATION - LEVITATION OBSERVATION OF DENDRITE EVOLUTION IN STEEL TERNARY ALLOY RAPID SOLIDIFICATION (LODESTARS)

**Merton C. Flemings[1]**, **Douglas M. Matson[2]**, **Robert W. Hyers[3] and Jan R.Rogers[3]**

Massachusetts Institute of Technology [1], Tufts University [2], NASA-MSFC [3]

## Abstract

During rapid solidification, a molten sample is cooled below its equilibrium solidification temperature to form a metastable liquid. Once nucleation is initiated, growth of the solid phase proceeds and can be seen as a sudden rise in temperature. The heat of fusion is rejected ahead of the growing dendrites into the undercooled liquid in a process known as recalescence.

Fe-Cr-Ni alloys may form several equilibrium phases and the hypoeutectic alloys, with compositions near the commercially important 316 stainless steel alloy, are observed to solidify by way of a two-step process known as double recalescence. During double recalescence, the first temperature rise is associated with formation of the metastable ferritic solid phase with subsequent conversion to the stable austenitic phase during the second temperature rise. Selection of which phase grows into the undercooled melt during primary solidification may be accomplished by choice of the appropriate nucleation trigger material or by control of the processing parameters during rapid solidification. Due to the highly reactive nature of the molten sample material and in order to avoid contamination of the undercooled melt, a containerless electromagnetic levitation (EML) processing technique is used.

In ground-based EML, the same forces that support the weight of the sample against gravity also drive convection in the liquid sample. However, in microgravity, the force required to position the sample is greatly reduced, so convection may be controlled over a wide range of internal flows. Space Shuttle experiments have shown that the double recalescence behavior of Fe-Cr-Ni alloys changes between ground and space EML experiments. This program is aimed at understanding how melt convection influences phase selection and the evolution of rapid solidification microstructures.

## Introduction

Suppression of convection in microgravity has been shown to dramatically impact rapid solidification kinetics. Glicksman and Huang[1] observed that the orientation of the g-vector relative to the principal growth direction could affect both growth velocity and side branch morphology during dendritic growth of succinonitrile, a non-metallic analog system.

The effect of convection on nucleation has not been similarly demonstrated. The purpose of this program is to develop a database characterizing the transformation from ferrite to austenite in Fe-Cr-Ni alloys to understand of the effects of convection on time-dependent nucleation phenomena during rapid

*Corresponding author email:  douglas.matson@tufts.edu   **Principal Investigator

solidification from the melt. A ternary alloy system was chosen so that varying the composition allows independent control of thermal and solutal effects.

This research has application to the design of industrial welding, spray forming and strip casting operations for a commercially important class of structural materials. In addition, this research also addresses fundamental issues relating to rapid solidification behavior, metastable phase selection and analysis of the processes governing microstructural evolution. By mapping out how convection influences nucleation behavior we hope to provide insight into how to better control solidification structures. Experiments focus on the use of convection as a processing control parameter.

### Background
Classical nucleation theory predicts that the time-dependent nucleation rate, $I_t$, is a function of the steady-state nucleation rate, $I_s$ :

$$I_s = N \ k_n^{+} \ Z \ \exp \left( - \frac{\Delta G_n}{k_B \ T \ n_c^2} \ f(\theta) \right) \tag{1}$$

$$I_t = I_s \ \exp \left( -\frac{\tau}{t} \right) \tag{2}$$

$N$ is the number of nucleation sites, $k_n^{+}$ the rate of monomer addition to the critical nucleus, $Z$ the Zeldovich factor with $Z = [ \ \Delta G_n / 3 \ \pi \ k_B \ T \ ]^{\frac{1}{2}}$, $\Delta G_n$ the free energy of formation for the critical nucleus, $k_B$ the Boltzmann constant, $T$ the nucleation temperature, $n_c$ the number of atoms in the critical nucleus, the contact angle factor $f(\theta) = \frac{1}{4} ( \ 2+cos\theta \ )( \ 1-cos\theta \ )^2$ , $t$ the time and $\tau$ the characteristic incubation time[2]. Kantrowitz proposed an expression including the atomic diffusivity $D$:

$$I_t = 2N \left( \frac{D}{\pi \ t} \right)^{\frac{1}{2}} \exp \left( -\frac{n_c^2}{D \ t} \right) \tag{3}$$

valid for small times such that the time dependent nucleation rate is not appreciable until :

$$\tau = \frac{n_c^2}{D} \tag{4}$$

in agreement with Turnbull[3] for diffusivity across a liquid interface and with Russell[4] who introduced a factor of ten to correct for intrinsic bulk diffusivity during solid state transformations. Recent work by Kelton[5] has shown that the time-dependent nucleation rate is significantly longer in partitioning transformations when the interfacial attachment and diffusive transport are linked in a coupled-flux analysis approach. By including the effects of solute diffusion in nucleation theory, a theoretical framework is established to test how convection may influence transient nucleation phenomena.

Based on classical nucleation theory, the number of atoms in the critical nucleus is a function of the geometry of the process. Comparing a spherical nucleus to that for a cylindrical flat plate :

$$n_c^{sphere} = \frac{4}{3} \ \pi \ r_c^3 \ \propto \ \frac{C_{sphere}}{(\Delta T)^3} \tag{5}$$

$$n_c^{plate} = \pi \ r_c^2 \ \propto \ \frac{C_{plate}}{(\Delta T)^2} \tag{6}$$

for a critical nucleus radius of $r_c = \dfrac{2 \ \gamma \ T_m}{\Delta H \ (\Delta T)}$ with $\gamma$ the surface energy, $T_m$ the melting point, $\Delta H$ the heat of fusion, and $\Delta T$ the undercooling. Combining these results we see that for a spherical cap the characteristic delay time should be proportional to the undercooling to the negative sixth power while for a cylindrical flat plate the delay should be proportional to the undercooling to the negative fourth power.

Fe-Cr-Ni alloys may form several equilibrium phases and the hypoeutectic alloys, with compositions near the commercially important 316 stainless steel alloy, are observed to solidify by way of a two-step process known as double recalescence, shown in Figure 1. During double recalescence, the first temperature rise is associated with formation of the metastable ferritic solid phase with subsequent conversion to the stable austenitic phase during the second temperature rise[6,7]. This experimentally determined delay time is assumed to be analogous to the theoretically evaluated incubation time.
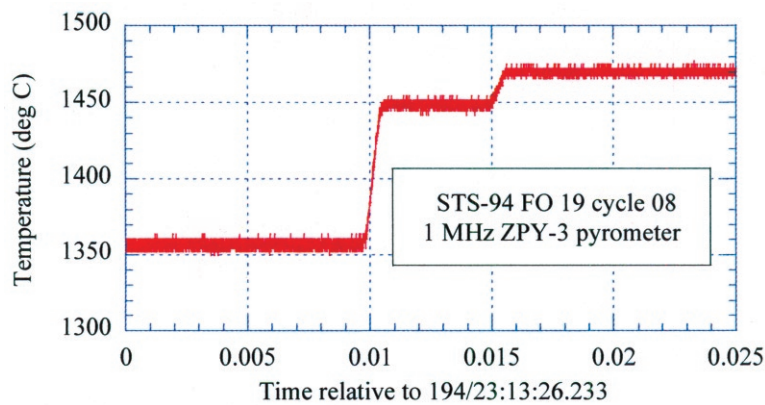


Figure 1. Double recalescence in ternary steel alloys processed in microgravity.

Ground-based research on levitation melted samples and on rapidly solidified atomized droplets has shown the strong influence of processing conditions on the selection between bcc-ferrite (delta) and the fcc-austenite (gamma) in Fe-Ni and Fe-Cr-Ni alloys. Early work on metastable formation in Fe-Ni alloys was accomplished by investigation of the solidification behavior of fine powders including the work of Cech[8] and Thoma and Perepezko[9]. Similar behavior was seen for commercial alloys both by Kelly and VanderSande for gas-atomized type 303 stainless steel[10] and by MacIsaac et al. in type 316 stainless steel[11] cooled in a glass matrix. The metastable phase formation was identified using a metallographic technique.

Solute-rich inversely cored structures in glass-encased bulk samples of Fe-Ni alloys were reported by Kattamis and Flemings[12] and Perepezko et al.[13] Remelting and coarsening during and immediately after recalescence was proposed by Abbaschian and Flemings[14] as mechanisms to explain the observed microstructure especially if the cooling rate was high[15]. The solidification path involved diffusionless rapid solidification to the equilibrium solidus or to the $T_o$-curve, a subsequent temperature rise to the completion of recalescence as described by the equilibrium phase diagram, and finally a decrease in temperature during slow equilibrium cooling. Coarsening defines the final observed dendrite arm spacing.[12]

At first, these inversely cored structures were assumed to represent the portion of solidification where solute trapping was important during the first rapid recalescence period but pyrometric evidence[6,16] and

metallographic evidence combined with concentration mapping of quenched steel samples by Koseki and Flemings[7,17] showed retention of the metastable bcc phase as shown in Figure 2. Calculations confirmed that the ferrite phase was more likely to nucleate from the melt based on differences in liquid-solid surface energy.
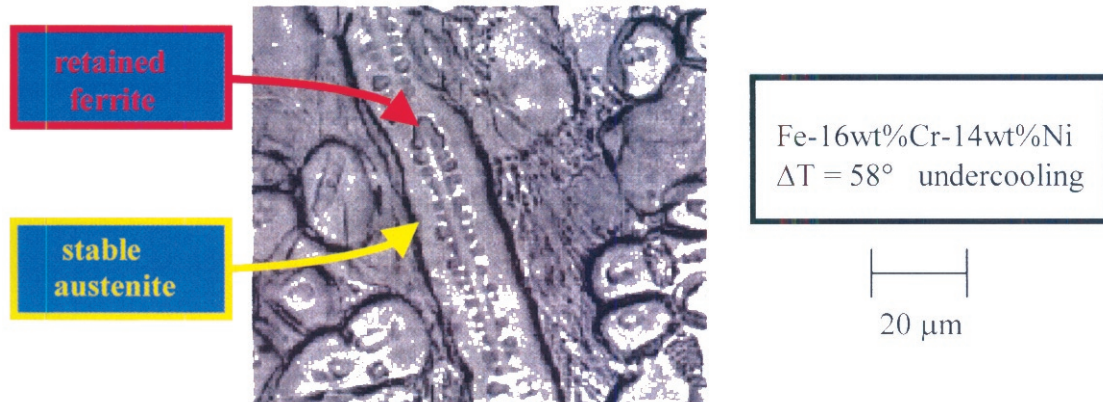


Figure 2. Retained metastable bcc core within fcc dendrites following rapid quenching of double recalescence in containerless processing of steel samples[7].

During double recalescence, both the intermediate temperature increase following primary recalescence and the delay between events is seen to be a strong function of composition. In separate investigations, Koseki and Flemings[6], Loser[18], Moir[19] and Volkmann[20-22] documented the relationship between growth kinetics, undercooling and composition.

Stainless steel alloys require special handling in order to achieve a significant undercooling range. In particular, chromium is particularly susceptible to contamination through reaction with crucible material. When attempting to perform rapid solidification tests, the formation of active heterogeneous nucleation sites limits the undercooling that may be achieved. A containerless technique minimizes this contamination.

Electromagnetic levitation (EML) is attractive as an experimental tool in these types of investigations because significant convection may be introduced into the melt[23]. The sample is positioned in the electromagnetic potential well generated by alternating current flowing through water-cooled copper coils. The eddy currents induced in the sample produce heat and levitate the sample. Induced currents also interact with the applied magnetic field to produce stirring forces inside the molten sample which lead to intense internal agitation, mixing and surface deformation. Quantification of induced flows is accomplished by magnetohydrodynamic modeling. Also, varying the sample size varies the Reynolds number independent of the absolute maximum melt recirculation velocity.

The same electromagnetic forces that position the sample also drive internal flow within the droplet. Since the electromagnetic force balances the weight of the sample, only a narrow range of convective conditions is accessible in 1-g EML. However, in microgravity, the positioning forces required to contain the sample are significantly weaker than on ground allowing the attainment of lower internal flow conditions. High force, high flow conditions may also be selected in microgravity and thus a wide range of convective environments may be accessed.

Previous testing in microgravity during the MSL-1 shuttle mission showed significant difference from the solidification behavior observed in ground-based EML experiments. Although growth rate measurements show no significant difference in behavior, the delay between primary recalescence and nucleation of the stable phase was approximately four times longer in microgravity[24,25] as shown in Figure 3. Data points taken during MSL-1R are shown in red and compared to results obtained in ground-based EML experiments both at MIT and at IFW-Dresden as shown in blue. This deviation was attributed to differences in convection conditions encountered on ground and in microgravity.
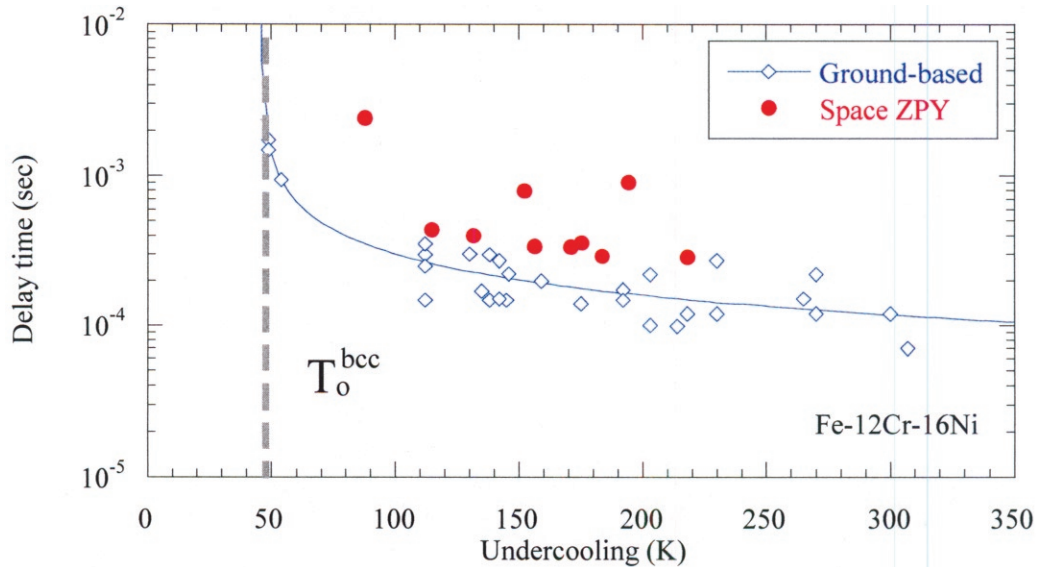


Figure 3. Delay between recalescence events.

## Flight Preparations

### Evaluation of Thermodynamic Driving Force

In a binary alloy system, solute concentration and corresponding thermal driving force which controls subsequent transformations are set by the equilibrium phase diagram. If a ternary alloy is used, the solute composition may be carefully adjusted to yield the same thermal driving force for different solute concentrations. Kertz[26] is investigating the growth of the stable phase into the metastable array in ground-based investigations. The equilibrium phase diagram, metastable phase diagram and thermodynamic properties can be evaluated over the entire family of ternary alloys using the software package ThermoCalc (Royal Institute of Technology, Stockholm Sweden). From these results, the thermal driving force may be approximated as the difference in $T_o$ temperatures for each phase (since this represents the temperature difference between metastable and stable phases, or undercooling, following primary recalescence).

$$\Delta T_o = T_o^{fcc} - T_o^{bcc} \qquad (7)$$

As shown in the left side of Figure 4, the right side of the figure presents two isopleth sections of the calculated metastable phase diagram. The figure shows how alloys of dissimilar constitution may be selected to obtain similar thermal driving forces; this ability to isolate effects of solute and thermal driving forces is the key attribute for selection of a ternary alloy system.

As shown in Figure 5, a plot of the delay times for various alloys as a function of the thermal driving force $\Delta T_o$ shows a slope of m = (-4.0) indicating that nucleation of the stable phase occurs as a flat plate on the pre-existing metastable skeleton.
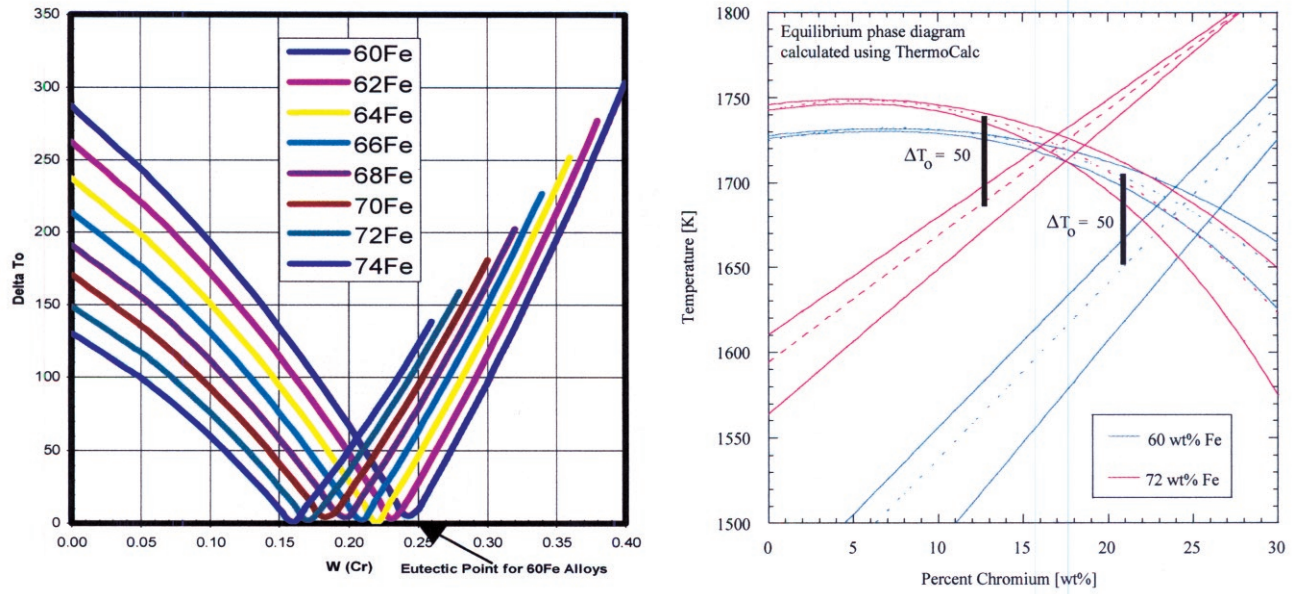
225

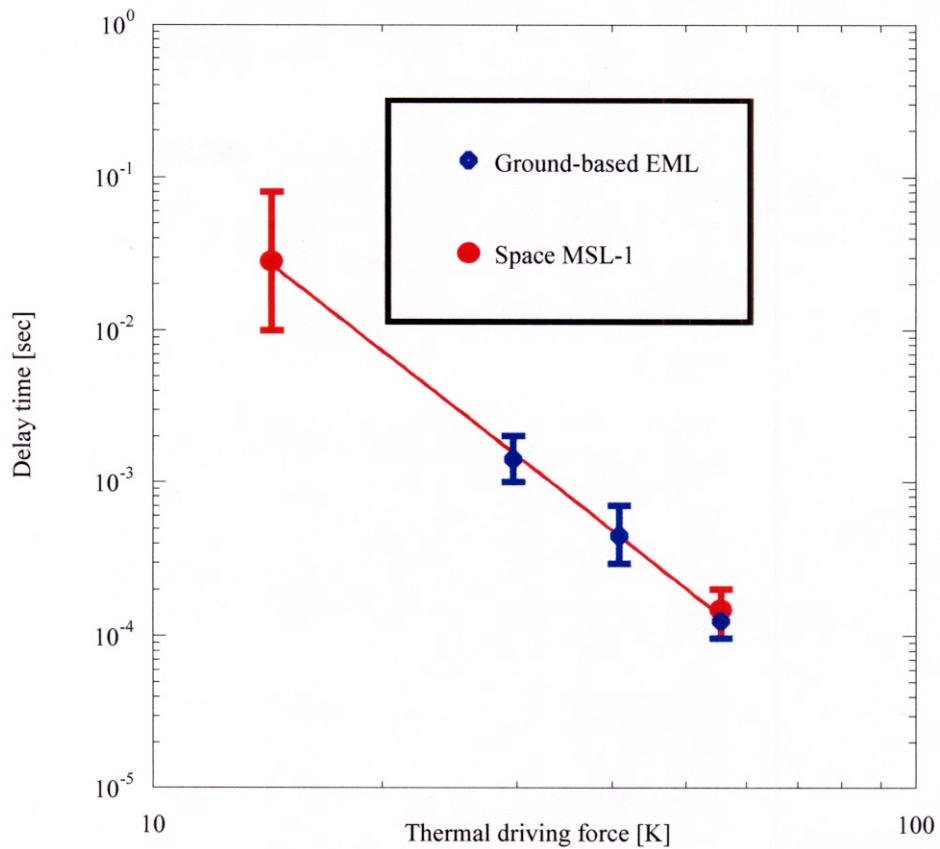Figure 4.  Thermal driving force and alloy selection.



Figure 5.  Thermal driving force and delay time; the bars show the variation due to convection and to the
initial undercooling which determines the initial fraction solid.

*Electromagnetic Levitation (EML) Testing*
EML testing as part of ongoing thesis work at MIT by Kensel[27] has shown that alloys with similar thermal driving force have similar delay time behavior. Figure 6 shows that the alloys with 50 degree driving force (as depicted in Figure 4) have comparable delay times. The general shape of this curve can be predicted from classical nucleation theory when combined with a simplified model of how rapid solidification progresses as a function of undercooling. In this model, undercooling during primary solidification results in a defined quantity of metastable fraction solid as predicted by the Stefan equation:

$$f_s^\delta \, \Delta H_{bcc} \; = \; C_p \, \Delta T_\delta \qquad\qquad (8)$$

where $f_s^\delta$ is the fraction solid of the primary metastable delta-phase, $\Delta H_{bcc}$ the latent heat of fusion, $C_p$ the heat capacity and $\Delta T_\delta$ the undercooling relative to the metastable phase diagram.
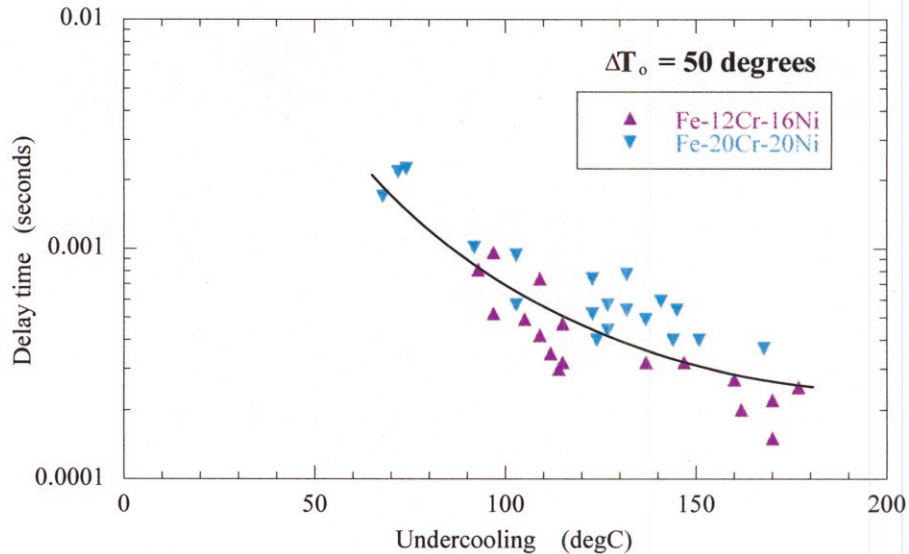


Figure 6. Delay time as a function of undercooling.

From the equilibrium phase diagram, the lower the initial undercooling, the lower the fraction solid that must result, and the higher the primary recalescence temperature (from application of the lever rule). This effect will be pronounced at low undercoolings but as primary undercooling is increased and growth velocity for the metastable phase becomes rapid, deviation from the equilibrium phase diagram is expected.

*Electrostatic Levitation (ESL) Testing*
ESL testing at NASA Marshall Space Flight Center (MSFC) has centered on evaluating the delay behavior over the range of recirculation velocities accessible using Marangoni or surface tension driven flow. Since the ESL achieves containerless processing by imposing a voltage drop across the sample processing space and levitation occurs through electrostatic attraction (similar to classic experiments by R.A. Millikan on oil drops), the sample size for ESL testing is much smaller than that used in EML tests. ESL samples are around 1 mm in diameter while EML samples are between 6-10 mm. When the sample is free-cooled with the heating laser turned off, recirculation within the droplet quickly dampens to near zero velocity conditions.

In ESL processing, the cooling rate may be controlled by operating the heating laser at reduced power. Processing with the laser on also induces temperature differences across the sample surface and thus

surface tension driven flows result. ESL processing of Fe-Cr-Ni alloys gives laminar flow in the range of 0 – 6 cm/sec while EML processing on ground results in turbulent flow at about 32 cm/sec. Figure 7 shows a comparison between tests performed using the MSFC-ESL with the laser off and the laser on. The difference between the observed delay time for these two conditions is not statistically significant.
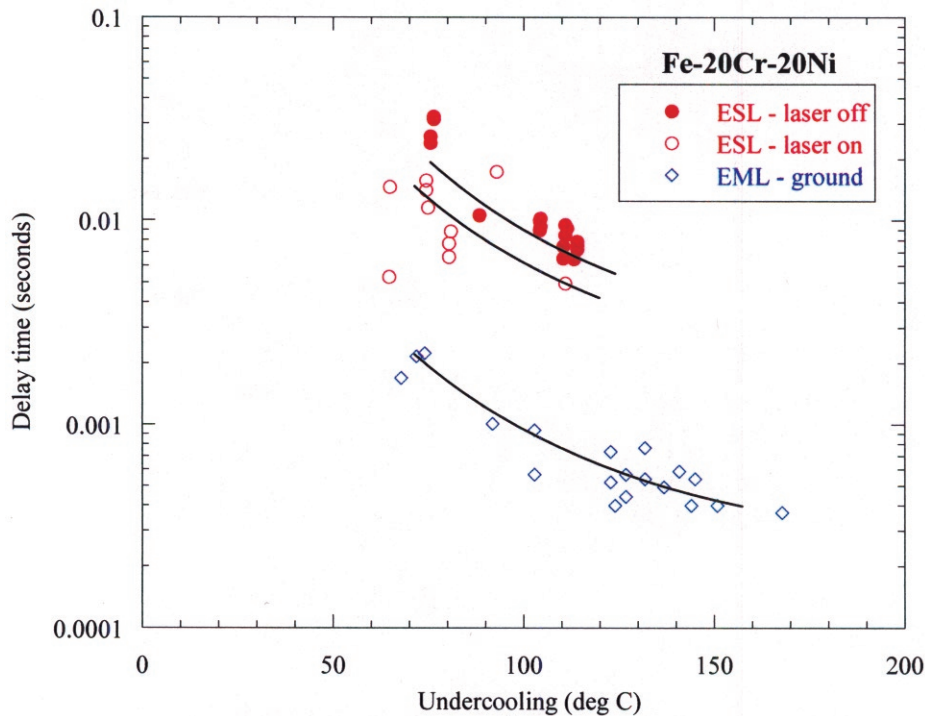


Figure 7. Comparing EML and ESL test results.

By comparison, ground-based EML testing on the same alloy composition yield results which vary significantly from the ESL delay times. All data sets show the same trend – delay times under high convective conditions are significantly shorter.

### Justification for conducting experiments in microgravity
Due to the highly reactive nature of the molten sample material and in order to avoid contamination of the undercooled melt, a containerless processing technique must be used. Since the goal of the project is to investigate the role of convection in phase selection, we desire the ability to induce a range of known, steady-state levels of convection during rapid solidification processing. The range of flows to be explored must focus on the range of velocities between the extremes identified during the previous MSL-1 testing. Of particular interest is the behavior during transition from laminar to turbulent flow.
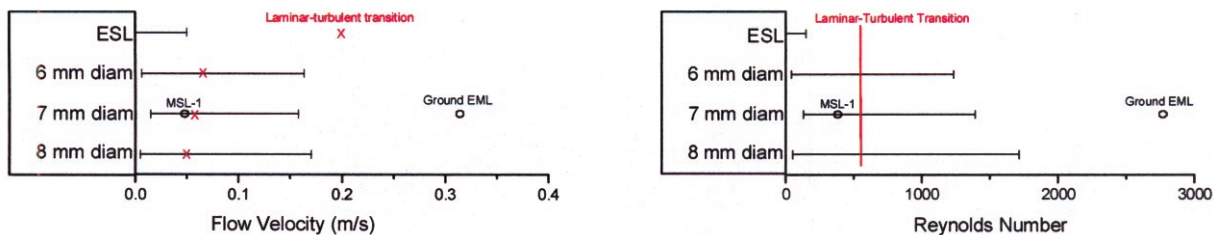


Figure 8. Comparison of the range of recirculation velocities and Reynolds numbers accessible using space- based EML to other experimental platforms[28].

Figure 8 shows a comparison of ground-based experimental platforms to that achievable using space-based EML. ESL testing can only access a laminar flow range from $0 < V_{max} < 6$ cm/sec while ground-based EML is limited to turbulent flow corresponding to a condition where $V_{max}$ is on the order of 32 cm/sec. Results from MSL-1 show that the significant change in nucleation behavior occurs <u>between</u> these two extremes (note that the ESL and MSL-1 results are of similar magnitude and correspond to laminar flow conditions). Only microgravity EML can access a majority of the full range and investigate the laminar/turbulent flow transition.

**Summary**
From high-speed digital images of the double recalescence behavior of Fe-Cr-Ni alloys in ground-based testing and in reduced gravity aboard the NASA KC-135 parabolic aircraft, we have shown that phase selection can be predicted based on a growth competition model. An important parameter in this model is the delay time between primary nucleation and subsequent nucleation of the stable solid within the liquid / metastable solid array. This delay time is a strong function of composition and a weak function of the undercooling of the melt below the metastable liquidus.

From the results obtained during the MSL-1 mission and in ground based electrostatic levitation testing at NASA Marshall Space Flight Center (MSFC), we also know that convection may significantly influence the delay time, especially at low undercoolings. We know that for ternary alloys with a similar thermal driving force, the nucleation delay is comparable; this contrasts with the observation that for a single alloy, different nucleation delays are seen under different convective conditions.

Currently, it is unclear what mechanism controls the formation of a heterogeneous site that allows nucleation of the austenitic phase on the pre-existing ferritic skeleton. By examining the behavior of the delay time under different convective conditions attainable in microgravity, we hypothesize that we can differentiate among several of these mechanisms to gain an understanding of how to control microstructural evolution.

**References**
1. Glicksman, M. E., Huang, S. C., In: Proc. 3rd European Symposium on Materials Science in Space, ESA SP-142, Grenoble, 309, (1979).
2. Kantrowitz, A., J. Chem. Phys. **19**, 1097, (1951).
3. Turnbull, D., Solid State Physics, **3**, 225, (1956).
4. Russell, K.C., Acta Met., **16**, 761, (1968).
5. Kelton, K.F., "Time-Dependent Nucleation in Partitioning Transformations", Acta Mat. **48**, 1967 (2000).
6. Koseki, T. and Flemings, M.C., Met. Trans., 26A, 2991, (1995).
7. Koseki, T. and Flemings, M.C., Met. Trans., 27A, 3226, (1996).
8. Cech, R.E., Trans. AIME, **206**, 585, (1956).
9. Thoma, D.J. and Perepezko, J.H., Met. Trans., **23A**, 1347, (1992).
10. Kelly, T.F. and VanderSande, J.B., Int. J. Rapid Solidification, **3**, 51, (1987).
11. MacIsaac, D. G., Shiohara, Y., Chu, M. G., and Flemings, M. C., in Grain Refinement in Castings and Welds, ed. Abbaschian, G. J. and David, S. A., Met. Soc. of AIME, 87, (1983).
12. Kattamis, T. Z. and Flemings, M. C., Trans. AIME, **236,** 1523, (1966).
13. Perepezko, J. H., Shiohara, Y., Paik, J. S., and Flemings, M. C., in Rapid Solidification Processing: Principles and Technologies, III, ed. Mehrabian, R., National Bureau of Standards, 28, (1982).

14. Abbaschian, G. J. and Flemings, M. C., Met.Trans., **14A**, 1147, (1983).
15. Flemings, M. C., and Shiohara, Y., Materials Science and Engineering, **65**, 157, (1984).
16. Zhao, Q., Piccone, T. J., Shiohara, Y., and Flemings, M. C., in Rapid Quenching and Powder Preparation, Tokyo, Japan: MRS Int. Meeting on Adv. Mat. v. 3, 597, (1989).
17. Koseki, T. and Flemings, M. C., Met. Trans., **28A**, 2385, (1997).
18. Löser, W., Volkmann, T., and Herlach, D.M., Mater. Sci. Engr., **A178**, 163, (1994).
19. Moir, S. and Herlach, D.M., Acta Metall., **45**(7), 2827, (1997).
20. Volkmann, T., Löser, W., and Herlach, D.M., Int. J. Thermo., **17**(5), 1217, (1996).
21. Volkmann, T., Löser, W., and Herlach, D.M., Met. Trans., **28A**, 453, (1997).
22. Volkmann, T., Löser, W., and Herlach, D.M., Met. Trans., **28A**, 461, (1997).
23. Trapaga, G., Matson, D. M., Hyers, R. W., and Flemings, M. C., in Proceedings of the Julian Szekely Memorial Symposium on Materials Processing, Sohn, H. Y., Evans, J. W., and Apelian, D., eds., TMS Warrendale PA, 453, (1997).
24. Flemings, M. C. and Matson, D. M., in NASA/CP 1998-208868, Robinson, M. B., ed., NASA-MSFC AL, 281, (1998).
25. Matson, D. M., Löser, W., and Flemings, M. C., in Solidification 1999, Hofmeister, W. H., Rogers, J. R., Singh, N. B., Marsh, S. P., and Voorhees, P. W., eds., TMS Warrendale PA, 99, (1999).
26. Kertz, J. E., and Matson, D. M., "Measurement of Steel Growth Kinetics using TEMPUS Aboard the NASA KC-135 Parabolic Aircraft", Proceedings of the First International Symposium on Microgravity Research Applications, ESA SP-454, 639, (2001).
27. Kensel, L., MIT SM-thesis, 2002 – in progress
28. Hyers, R. W., personal communication, (2002).